Published in final edited form as:
Conf Proc IEEE Eng Med Biol Soc. 2012 ; 2012: 1405–1408. doi:10.1109/EMBC.2012.6346202.

Swept Source Optical Coherence Tomography based Smart Handheld Vitreoretinal Microsurgical Tool for Tremor Suppression

Cheol Song,
Department of Electrical and Computer Engineering, Johns Hopkins University, Baltimore, MD 21218 USA

Peter L. Gehlbach, and
Director of Retina Training at the Wilmer Eye Institute, Johns Hopkins University School of Medicine, Baltimore, MD 21218 USA

Jin U. Kang
Department of Electrical and Computer Engineering, Johns Hopkins University, Baltimore, MD 21218 USA

Cheol Song: csong16@jhu.edu; Peter L. Gehlbach: pgelbach@jhmi.edu

Abstract

Microsurgeons require the ability to make precise and stable maneuvers in order to achieve surgical objectives and to minimize surgical risks during freehand microsurgical procedures. This work presents a novel common path swept source optical coherence tomography based smart surgical tool that suppresses hand tremor. It allows enhanced tool tip stabilization, more accurate targeting and may lower surgical risk. Here the one dimensional motion tremor of a surgeon's hand is assessed by the surgical instrument. The ability to accurately locate a surgical target and the ability to maintain tool tip offset distances in a chicken embryo model are significantly improved as compared to freehand use.

I. Introduction

Micro-surgeons may have hand tremor on the order of 50–100 microns [1]. Retinal surgery such as 3-port pars plana vitrectomy requires precise fine motor control to achieve surgical objectives and to reduce surgical risks [2–3]. Unintended surgeon, instrument or patient movement can result in ocular injury and difficulty in performing critical surgical tasks. Some fine micro-manipulations are still beyond the motor control of even the best surgeons. To assist a surgeon's in performing micron scale maneuvers, various approaches have been developed: Johns Hopkins "Steady Hand" robots [4–5], handheld microsurgical robot, Micron [6–7], and other active handheld steady-hand and robot-assisted schemes [8–9].

Since 1991, optical coherence tomography (OCT) has emerged as a highly useful ocular imaging modality. Functional application of the OCT signal is being rapidly developed [10–11]. OCT technology has recently been utilized as a distance sensor or force sensor, by using common path optical coherence tomography (CP-OCT) [12–13]. The CP-OCT based surface topology and motion tracking system [14] and a conceptual surgical tool for micro-incision [15] have recently been presented. The instruments presented were however not fully functional handheld tools. Here we propose a method by which to compensate for surgeon hand tremor and unintended instrument drift. The design and implementation of a novel handheld surgical tool using a common path swept source optical coherence tomography (CP SS-OCT), and data comparing freehand and smart tool assisted task

performance are presented. In this study, the active compensation capabilities of the surgical tool are evaluated. The tool's ability to maintain constant offset distances is analyzed during free-hand use in dry phantoms and in a chicken embryo model.

II. METHODS

A. Smart Handheld Surgical Tool

This work proposes the design and basic implementation of a CP SS-OCT based a smart handheld surgical tool for distance sensing combined with a piezoelectric motor for the tremor and drift compensation. The ergonomics of this first-generation prototype is based on a commercial product that is currently used in retinal surgery. The main components of the surgical tool are the piezoelectric motor (LEGS-L01S-11, PiezoMotor) and two commercial syringe needles (20-gauge and 25-gauge, BD syringe). The tool design considers various important factors in its assembly and performance.. Four separated parts (front holder, back holder, tail, and joint) were manufactured for convenient assembly. As shown in Fig. 1(a), two lure-lock hypodermic needles for easy combination with the front holder and motor shaft are introduced. The inner needle is attached to the motor shaft while the outer needle is connected into the front holder. The outer needle functions as a movement guider of the inner needle. The motor inside the back holder is fixed by mechanical components. The size of the motor (22 mm × 10.8 mm × 18.7 mm) determines the minimum cross- sectional area of the tool. The piezoelectric motor with bare metal has a maximum speed of 20 mm/s, maximum stroke of 55 mm, maximum force of 6.5 N, and a resolution of less than 1 nm. The joint part works as a medium which has a small hole for the single mode fiber for OCT signal detection. It also works as a connector for the inner needle and lure-lock screw connection. The front holder has enough inner space to allow the inner needle to move back and forth 12 mm. Fig. 1(a) depicts a transparent CAD of the tool. Fig. 1(b) shows the optical image of the smart surgical tool after finishing the assembly. The tool has a length of 140 mm excluding the surgical needle and a weight of about 65 g, including the motor weight of 20 g.

B. Closed-loop Control of CP SS-OCT based Microsurgical Tool

The swept source optical coherence tomography (SS- OCT) is composed of a swept source (Axsun technology), an optical isolator and a photodetector. The swept source has a sweep repetition rate of 50 kHz and a center wavelength of 1310 nm and a bandwidth of 110 nm providing an axial resolution of 16 μm, experimentally. The spectral interference detected by a photodiode is transferred into the workstation by a high-speed digitizer (AlazarTech, ATS9350), with one frame composed of 100 A-lines. The dual channel digitizer can achieve real-time acquisition with a resolution of 12 bit and a sampling rate of 500 MS/s, with 8-lane PCI Express. A quad-core workstation (Dell, T7500) could achieve high-speed data processing with the digitizer for acquiring OCT signals and real-time closed-loop control using a motor controller (PMD 90) and system software written in the Labview environment.

As shown in Fig. 2(a), the piezoelectric motor based PID controller operates the feedback loop with an update speed of 500 Hz to hold the target height of the surgical needle, which contains a single mode fiber for sensing the distance between the needle tip and a sample. Fig. 2(b) illustrates the schematic of the PID feedback control. Before acquiring the OCT signal, the inner surgical needle is always initialized at the center of the travel range of 12 mm. In order to search for the first sample surface, an edge detection scheme is applied to the control loop and the motor compensation starts to work only when the magnitude of OCT signal exceeds a predetermined threshold. To control the motor shaft moving the inner needle into the target height, the feedback control loop utilizes two motor parameters, the

velocity and the step size, which are determined by a function of the real-time height error. When the surgeon is holding the tool still or moving laterally, the feedback control system is applied to keep the constant offset from the chicken embryo. The stabilized fiber-optic based surgical tool would allow for automated surgical tool actions from a defined offset height.

III. RESULTS

A. Tremor Measurement with Freehand Use

The surgeon's hand tremor was measured by using the smart surgical tool without the compensation mode. The characteristics of the freehand tremor provided the reference signal to which compensation was applied. Two cases of hand tremor were measured by the tool. At first, the hand tremor while holding still during a longer time period (30 sec.) were compared with a shorter time period (5 sec.). As shown in Fig. 4(a), the tremor drift for a long-time period is larger than 100 μm from the target height of 1000 μm. Each average of two periods was 1013.14 μm (5 sec.) and 1005.66 μm (30 sec.), respectively. Each root mean square error of two periods is 36.04 μm (5 sec.) and 43.43 μm (30 sec.), respectively. In frequency analysis, the tremor frequency for short time is more broadly distributed, and the two frequency bands of 0–2 Hz and 8–12 Hz are relatively higher than the others.

We performed the 1000 micron sweep movement by looking at the screen and moving the instrument until the tracing was close to the target with the screen delay in place. The tool tip was moved repetitively from 1000 μm to 2000 μm for 15 second, the target height error was large and therefore the travel range was not same with each sweep. The average distance was 1766 μm and the maximum and minimum distances were 2761.9 μm and 1034.4 μm, respectively. In frequency analysis, the magnitude of the low frequency band of 0–2 Hz is higher than others due to the movement itself, particular at the frequency of 0.7 Hz.

B. Motion Compensation with Smart Surgical Tool

By analyzing the hand tremor of a retina surgeon, the smart surgical tool system with a closed-loop control using edge-searching algorithms for real-time depth tracking was able to effectively dampen unintended tool motion, while the motion compensation function may provide extended surgical capabilities. The tool is shown to be effective at tissue offset distance between 1 mm and 4 mm from the sample surface. The steady hand experiments were performed on a dry phantom and in a live chicken embryo model. Tool performance on the dry phantom was comparatively better with regard to position accuracy due in large part to the fact that there is no target motion to compensate for in the dry phantom model. A significant limitation of the tool at this stage of development and hence some of our data collection is the very limited tolerance to off precisely perpendicular data collection. In the case of the dry phantom model as shown in Fig 4, involuntary hand tremor of around 0–15 Hz is significantly reduced as compared to freehand use. The enhanced performance due to motion compensation is most evident in the low frequency band of less than 5 Hz. Also, the capability of maintaining a steady target height at 1000 μm during a 5 second interval is enhanced by hand tremor suppression. The average distances are 1013.14 μm (freehand) and 999.68 μm (compensation), respectively. Each root mean square error of two periods is 36.04 (freehand.) and 5.35 μm (compensation), respectively.

The motion compensation of the tool was also demonstrated in a chicken embryo model that provided a wet biological environment to assess tool function. Fig 5(a) illustrates the optical images of the chicken embryo model and the surgical needle on it. Fig 5(b) shows the comparison between freehand use and compensation results on chick embryo's membrane. The average of freehand and compensation modes were 990.85 μm (freehand) and 999.2 μm (compensation), respectively. The RMSEs were 63.82 μm (freehand) and 9.23μm

(compensation), respectively. The live chicken embryo target moves thereby simulating an important variable in the surgical environment. The smart surgical tool's compensation system provided increased tool stability when assessing the task of maintaining a constant stand-off height from the chick embryo's membrane as compared to freehand use.

IV. Conclusion

This work presents the initial design and early testing of a novel handheld surgical tool. The tool consists of a common path swept source optical coherence tomography based tool prototype that is assembled in aluminum housing. In first application the tool is used to analyze one dimension of a surgeon's hand tremor. In second application the tool utilizes its compensation system consisting of a closed-loop control, using edge-searching algorithms, for real-time depth tracking, limitation of tool motion, and motion compensation via a piezoelectric motor to "sense" and dampen involuntary physiological hand tremor of around 0–15 Hz, particularly in the low frequency band

This first generation tool is intended to serve as a core platform for a set of novel surgical tools that couple active OCT sensing and motion compensation technology into handheld microsurgical instruments. Potential added clinical value may derive from more accurate instrument targeting, novel micron scale tool actions, and minimization of surgical risk, novel microsurgical teaching approaches and enhanced surgeon capabilities.

Acknowledgments

Research supported by the U.S. National Institute of Health and National Eye Institute (NIH/NEI) Grant R01EY021540 and Research to Prevent Blindness (RPB).

References

1. Riviere C, Gangloff J, Mathelin M. Robotic Compensation of Biological Motion to Enhance Surgical Accuracy. Proc Of the IEEE. 2006; 94(9):1705–1716.
2. Horio N, Horiguchi M, Yamamoto N. Triamcinolone-Assisted Internal Limiting Membrane Peeling During Idiopathic Macular Hole Surgery. Arch Ophthalmol. 2005; 123:96–99. [PubMed: 15642818]
3. Murthy RK, Chalam KV. Assistant-Independent OptiFlex System for Contact and Noncontact Wide-Angle Viewing in Vitreoretinal Surgery. Arch Ophthalmol. 2010; 128:490–492. [PubMed: 20385947]
4. Taylor R, Jensen P, Whitcomb L, Barnes A, Kumar R, Stoianovici D, Gupta P, Wang Z, de Juan E Jr, Kavoussi L. A steady-hand robotic system for microsurgical augmentation. Int J Robot Res. 1999; 18:1201–1210.
5. Balicki M, Uneri A, Iordachita I, Handa J, Gehlbach P, Taylor R. Micro-force Sensing in Robot Assisted Membrane Peeling for Vitreoretinal Surgery. Med Image Comput Assist Interv. 2010; 13(Pt 3):303–310.
6. Becker BC, MacLachlan RA, Lobes LA Jr, Riviere CN. Semiautomated intraocular laser surgery using handheld instruments. Lasers Surg Med. 2010; 42:264–273. [PubMed: 20333740]
7. MacLachlan RA, Becker BC, Cuevas Tabarés J, Podnar GW, Lobes LA Jr, Riviere CN. Micron: an actively stabilized handheld tool for microsurgery. IEEE Trans Robot. 2012; 28:195–212. [PubMed: 23028266]
8. Bose B, Kalra AK, Thukral S, Sood A, Guha SK, Anand S. Tremor compensation for robotics assisted microsurgery. Proc 13th Annu Int Conf IEEE Biomedical Engineering Society. 1992; 3:1067–1068.
9. Ueta T, Yamaguchi Y, Shirakawa Y, Nakano T, Ideta R, Noda Y, Morita A, Mochizuki R, Sugita N, Mitsuishi M, Tamaki Y. Robot-assisted vitreoretinal surgery. Opthamology. 2009; 116(8):1538–1543.

10. Huang D, Swanson EA, Lin CP, Schuman JS, Stinson WG, Chang W, Hee MR, Flotte T, Gregory K, Puliafito CA, Fujimoto JG. Optical coherence tomography. Science. 1991; 254(5035):1178–1181. [PubMed: 1957169]

11. Song C, Ahn M, Gweon D. Polarization-sensitive spectral domain optical coherence tomography using a multi-line single camera spectrometer. Opt Express. 2010; 18(23):23805–23817. [PubMed: 21164725]

12. Kang JU, Han J, Liu X, Zhang K, Song CP. Endoscopic Functional Fourier Domain Common Path Optical Coherence Tomography for Microsurgery. IEEE J of Select Topic in Quantum Electron. 2010; 16(4):781–792.

13. Liu X, Iordachita I, He X, Taylor R, Kang J. Miniature fiber-optic force sensor based on low-coherence Fabry-Pérot interferometry for vitreoretinal microsurgery. Biomed Opt Express. 2012; 3(5):1062–1076. [PubMed: 22567596]

14. Zhang K, Kang JU, et al. A Surface Topology and Motion Compensation System for Microsurgery Guidance and Intervention Based on Common-Path Optical Coherence Tomography. IEEE TBME. 2009; 56(9):2318–232.

15. Zhang K, Kang JU. Common-path low-coherence interferometry fiber-optic sensor guided microincision. J Biomed Opt. 2011; 16:095003. [PubMed: 21950912]

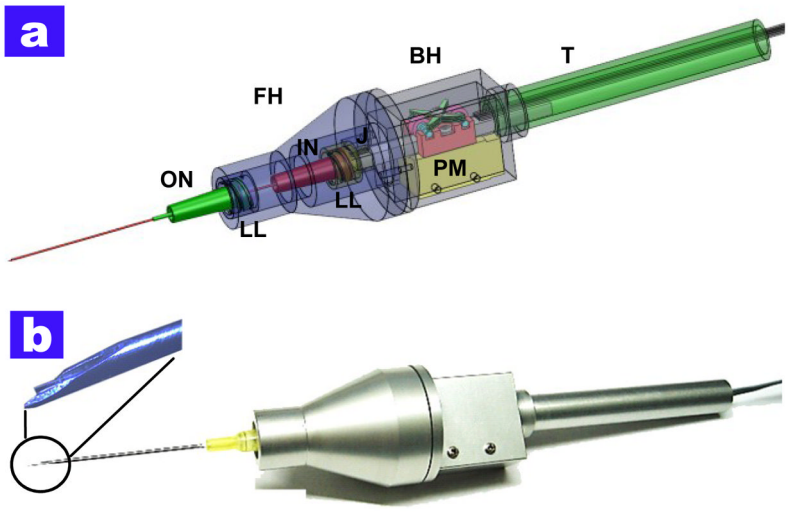

Fig. 1.

Smart surgical tool (a) computer rendering of the design of the tool. FH: front holder, BH: back holder, J: joint, T: tail, ON: outer needle, IN: inner needle, PM: piezoelectric motor, LL: luer-lock combination (b) the photo image after completing the assembly procedures

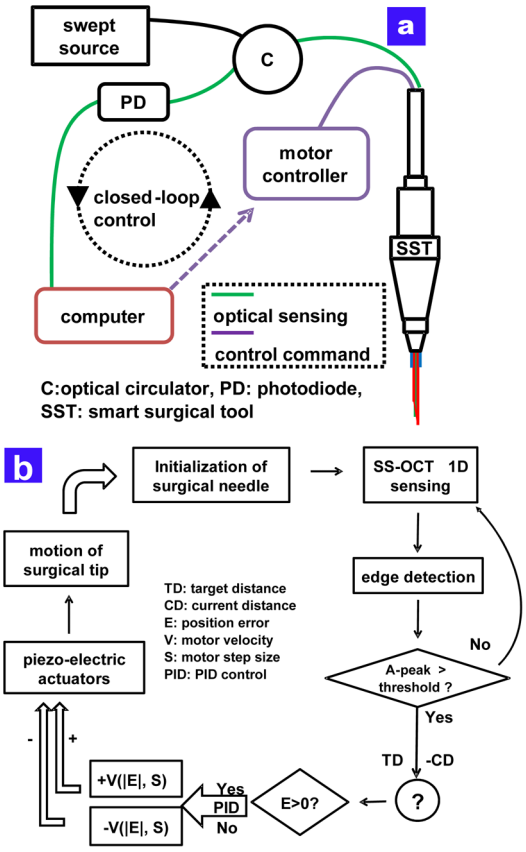

Fig. 2.

The feedback control scheme of the smart surgical tool (a) feedback control schematic of the common path SS-OCT based surgical tool (b) detailed PID based control scheme.

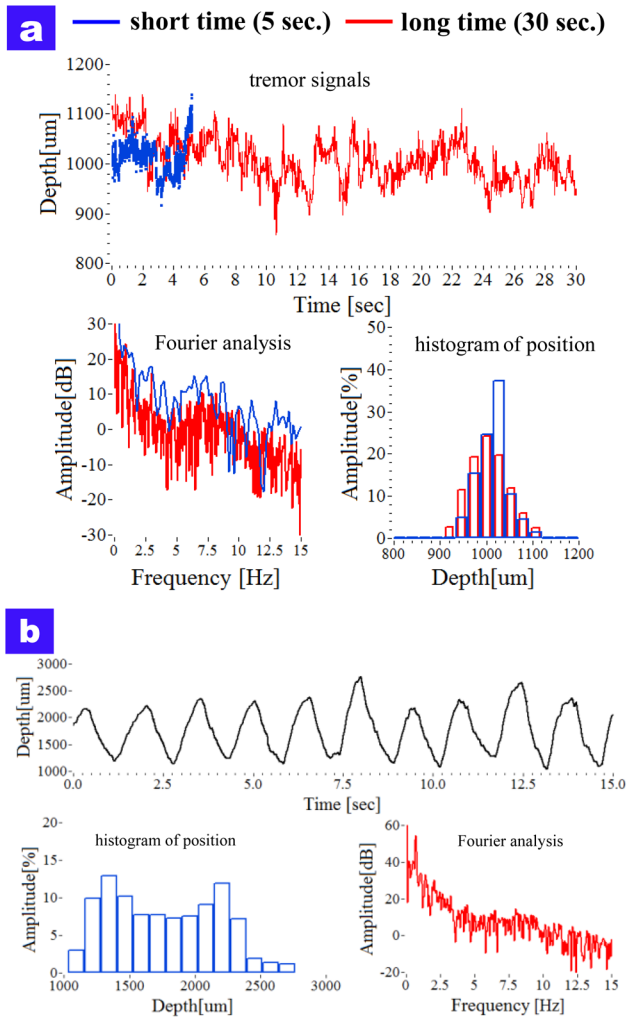

Fig. 3.

The characteristics of surgeon tremor with freehand use (a) attempting to hold steady at a defined offset height (b) swing the tool at offset height between 1000 μm and 2000 μm

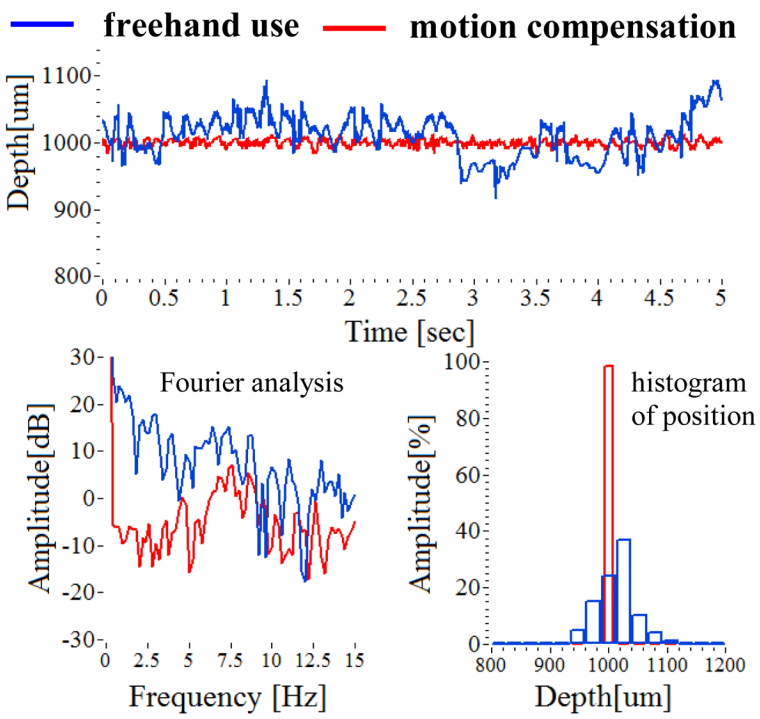

Fig. 4.

Comparison of freehand use and motion compensation of holding still at a offset height of 1000 μm from the dry phantom.

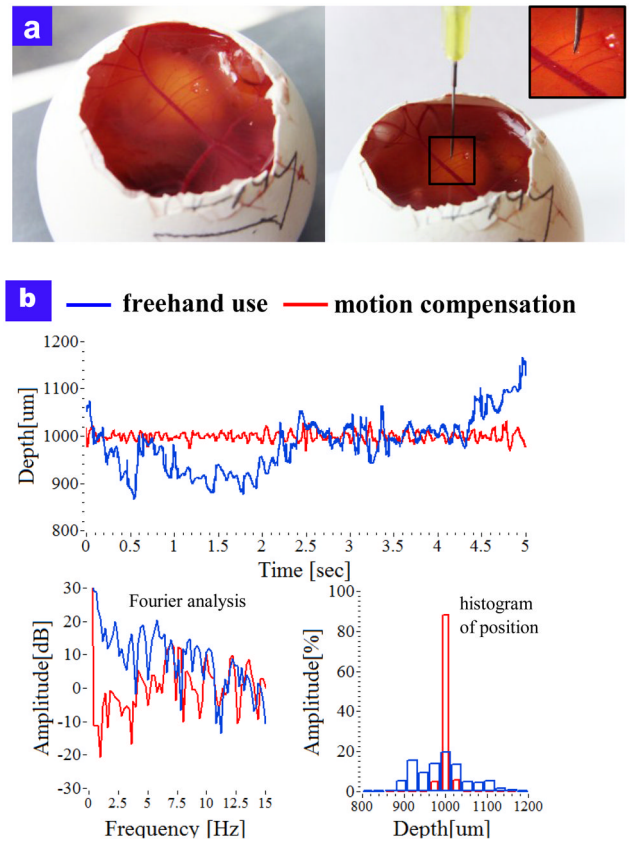

Fig. 5.

Motion compensation in chicken embryo model (a) photo image of live chicken embryo model (b) Comparison of free hand tool motion and tool motion with tremor suppression.